Supporting Information

Switching the adsorption sites of PMS on $SrCoO_{2.52}$ to enhance catalytic performance

Dan Yu[a,b], Jiahong He[b*], Taiping Xie[a,c], Qiang Xu [b], Houyang Chen[d,e], Bin Xiang[a*]

[a] School of Chemistry and Chemical Engineering, Chongqing University, Chongqing 400044, China.

[b] Chongqing Key Laboratory of Environmental Materials & Remediation Technologies, College of Chemistry and Environmental Engineering, Chongqing University of Arts and Sciences, Chongqing 402160, China.

[c] Chongqing Preschool Education College, Chongqing 404047, China.

[d] Chongqing Institute of Green and Intelligent Technology, Chinese Academy of Sciences, Chongqing 400714, China

[e] Chongqing School, University of Chinese Academy of Sciences, Chongqing 400044, China

* Correspondence: 20090005@cqwu.edu.cn (J. H. He), xiangbin@cqu.exu.cn (B. Xiang)

Texts

Text S1. Chemicals and Reagents.

All the reaction chemicals and reagents used in this study were analytical reagent (AR) or high-performance liquid chromatography (HPLC) grade. Peroxymonosulfate (PMS; $2KHSO_5 \cdot KHSO_4 \cdot K_2SO_4$), Potassium hydroxide (KOH), Potassium chloride (KCl), Potassium dihydrogen phosphate (KH_2PO_4), Potassium bicarbonate ($KHCO_3$), Potassium nitrate (KNO_3), Cobalt nitrate hexahydrate ($Co(NO_3)_2 \cdot 6H_2O$), Cobalt tetraoxide (Co_3O_4), Strontium nitrate ($Sr(NO_3)_2$), Sulfuric acid (H_2SO_4), Humic acid (HA), citric acid, Ethylene glycol, Tert-butyl alcohol (TBA), Benzoquinone (ρ-BQ), L-histidine, Ethylene Diamine Tetraacetic Acid (EDTA), and Enrofloxacin (ENR) were purchased from Sinopharm Chemical Reagent Co., Ltd. Methanol and acetonitrile were purchased from BCR International trading Co., Ltd. Deionized water was used throughout this study.

Text S2 Materials Characterization

The powder X-ray diffraction (XRD) technology was implemented on a Shimadzu 6100 instrument with Cu Kα X-ray radiation (λ= 1.5432 Å) in a range of 10 ~ 80°. Field emission scanning electron microscopy (SEM; Gemini SEM 500) was carried out at an acceleration voltage of 3 kV. Transmission electron microscopy (TEM) equipped with energy dispersive spectroscopy (EDS) were performed on JEOL JEM 2100F. X-ray photoelectron spectroscopy (XPS, Thermo Scientific K-Alpha) was applied with Al-Kα (hν = 1486.6 eV) as the radiation source and the binding energy was calibrated with C 1s = 284.80 eV binding energy standard. Electron paramagnetic resonance technology (EPR, Bruker EMXPLUS) was conducted to measure reactive oxygen species. 5,5-Dimethyl-1-pyrroline (DMPO) was used as the spin trapping agent for the detection of $^{\bullet}OH$, $SO_4^{\bullet-}$, and $O_2^{\bullet-}$ in aqueous solution. 2,2,6,6-tetramethyl-4-piperidone (TEMP) was employed as the spin trapping agent to monitor $^1O_2$. Inductively coupled plasma mass spectrometry (ICP-MS; Agilent 7800) was used to obtain the concentration of leached Sr and Co. Actual content of Sr and Co in raw and post-treated materials is also obtained by ICP-MS. Physisorption apparatus (Micromeritics ASAP

2460) is utilized to measure the specific surface area and pore structure of catalysts. Raman spectra were recorded on an HR Evolution Raman spectrophotometer (Horiba LabRAM) and scanned from 450 to 1500 cm^{-1} at a resolution of 1 cm^{-1} with 532 nm laser light irradiation. Nano particle size and zeta potential analyzer (DLS) were performed on Malvern Nano ZS90 and the zeta potential of catalyst was detected at different pH values. The total organic carbon (TOC) was determined by a TOC analyzer (Shimadzu TOC-LCPH).

The H_2 temperature-programmed reduction (H_2-TPR) was carried out on a Micromeritics AutoChem II 2920 instrument. 50 mg sample was placed in U-type quartz tube and dried at 200 °C for 1 h under a flow of He gas. Subsequently, the system was cooled down to 50 °C. Then, the sample was desorbed in a 10% H_2/Ar stream at a ramp rate of 10 °C/min to 700 °C and the reduction gas was detected by TCD detector.[1] The O_2 temperature programmed desorption (O_2-TPD) was also implemented on Micromeritics AutoChem II 2920 instrument. Prior to each analysis, the 80 mg sample was put in a quartz U-shaped reactor and dried at 200 °C for 1 h under a flow of He gas. Subsequently, the sample was cooled down to 50 °C and then a 10% O_2/He stream was passed through until saturated. Immediately, the He flow was introduced to remove weakly adsorbed O_2. Finally, the system was heated up to 700 °C (10 °C/min) under He gas and the O_2 desorption was detected by TCD detector.[2]

Text S3 Electrochemical Measurement

For the preparation of working electrode, 10 mg catalyst was dispersed in mixed solution including 20 μL of 0.5 wt% Nafion solution and 1 mL of deionized water, followed by ultrasonic treatment for 1 h. Subsequently, 10 μL slurry was dipped onto the polished glassy carbon electrode (3 mm in diameter) and dried at ambient condition. Electrochemical measurements were conducted on three-electrode system (CHI 660E). Ag/ AgCl (saturated KCl) electrode and platinum foil were used as reference electrode and counter electrode. The electrolyte was 0.1 M Na_2SO_4. Amperometric i−t curve measurements was carried out upon the addition of PMS and ENR at open circuit potential (OCP).[3]

Text S4 Analytical Methods of ENR and Intermediates

Ultra-high-performance liquid chromatograph (UPLC; waters) equipped with a PDA detector (271 nm) was applied to measure the concentration of ENR.[4] Reverse-phase C-18 column was carried out for chromatographic separation. 1.0 % acetic acid and acetonitrile with a volume ratio of 60:40 form a mobile phase at a flow rate of 0.3 $mL \cdot min^{-1}$. The injection volume was 10 μL and the temperature of chromatographic columns and samples were kept at room temperature.

High-resolution mass spectrometry (Q Exactive, Thermo Scientific, Bremen, Germany) was carried out to detect the intermediates of ENR. Hypersil column (GOLD C 18, 2.1 × 100 mm, 3.0 μm) was conducted to separate samples using acetonitrile (A) and 0.5% formic acid (B) as mobile phase.[5] The gradient began with 15% A at 0 min, where it was held for 1 min and then followed by an increase to 30% A at 4 min. In the next 2 min, it maintained at 70% A and finally arrived at 15% A at 12 min. The flow rate was remained at 0.2 $mL \cdot min^{-1}$ and the column oven temperature was kept at 30 °C. Orbitrap Mass Spectrometer analysis was implemented on electrospray ionization (ESI) positive ion mode and scan range of 50–1000 m/z.

Text S5 Performance Evaluation of ENR Degradation.

The experiment for ENR degradation was performed at room temperature with mechanical stirring. Firstly, 10 mg ENR was dissolved into 1L of deionized water. Then, 50 mL of ENR solution was measured and placed in three-neck round bottom. Afterwards, 5 mg of the catalyst was added into the solution and mechanically stirred for 30 min to establish the adsorption–desorption equilibrium. Finally, 200 μL 50 g/L PMS was added into suspension to start the reaction. At specific time intervals, 1 mL of mixture was withdrawn and immediately mixed with 100 μL methanol to quench any possible reaction. The catalyst was filtered through a 0.22 μm nylon filter membrane and the filtrate was collected into sample vials. The initial pH of this reaction system was around 6.5, and the pH was adjusted by diluted KOH and H_2SO_4. The used catalyst was recollected through by filtration, washing, and drying. Repeated

experiments were performed to prevent chance errors.

To further investigate the reaction kinetics of SCC-2/PMS system, the pseudo-first order kinetic model was introduced to describe the ENR degradation expressed as $\ln\left(\frac{C_0}{C_t}\right) = k_{obs}t$. ($C_0$ and C_t is the ENR concentration at initial and reaction time t, respectively; k_{obs} is the reaction rate constant; and t is the reaction time).

In order to reveal the relationship between the reaction rate constant and the reaction temperature, the apparent activation energy was calculated according to the Arrhenius formula: $k = Ae^{-\frac{E_a}{RT}}$ (k is the rate constant of the reaction at a temperature of T, R is the molar gas constant, A is the per-exponential factor, and E_a is the apparent activation energy).

In order to check the contributions of different reactive oxygen species to degrade ENR, quenching experiments were applied. Methanol (MeOH), tert-butyl alcohol (TBA), L-histidine, and benzoquinone (*p*-BQ) were added before reaction to quench $^{\bullet}OH$, $SO_4^{\bullet-}$, $^1O_2$, and $O_2^{\bullet-}$, respectively.

Effects of coexisting inorganic cations and natural organic matter on ENR degradation were investigated by first dissolving the corresponding substance in ENR solution before the reaction begins. Batch experiments were carried out at the typical condition: 50 mL 10 mg/L ENR, 0.2 g/L PMS, 0.1 g/L catalyst, and pH 6.5. To test the effect of coexisting Cl^-, NO_3^-, HCO_3^-, and $H_2PO_4^-$, 4 and 20 mM potassium salts were added.

Text S6 Performance Assessment of PMS Activation

The concentration of PMS was measured by high concentration iodometric method[6]. Absorbance was determined at a range of 450-290 nm using a UV-Vis spectrophotometer. Specifically, a coloring reagent of 0.1 $g \cdot mL^{-1}$ KI and 0.005 $g \cdot mL^{-1}$ $NaHCO_3$ was prepared and it was kept in the dark. The performance assessment of PMS activation was simply the replacement of ENR solution with deionized water at the typical condition. Finally, 0.5 mL of the suspension was taken out, filtered, and mixed with 20 mL coloring reagent. The reaction in the dark lasted 30 min.

Text S7 Computational Details

All calculations were carried out with CP2K package (version 7.1) in the framework of the density functional theory,[7] based on the hybrid Gaussian and plan-wave scheme.[8] Molecular orbitals of the valence electrons were expanded into DZVP-MOLOPT-SR-GTH basis sets, while atomic core electrons are described through Goedecker-Teter-Hutter (GTH) pseudopotentials.[9] A plane-wave density cutoff of 500 Ry was adopted. The long range van der Waals interaction is described by the DFT-D3 approach.[10] All the structures fully relaxed by CP2K with BFGS scheme, and the force convergence criterion was set to 4.5 * 10^{-4} hartree/bhor. The transition states of the decomposition of PMS were calculated by CI-NEB method.[11]

Text S8 Effect of Operating Parameters on ENR degradation

The dosage of SCC-2 was varied to explore the effect of catalyst dosage on ENR degradation in the SCC-2/PMS system. As the catalyst dosage was increased from 0.05 to 0.30 $g \cdot L^{-1}$, the ENR degradation efficiency increased from 81.12% to 100% within 3 min. The corresponding k_{obs} value increased from 0.441 to 2.302 min^{-1}, exhibiting a good linear relationship with the amount of catalyst. This may be due to that more catalysts provide more active sites, facilitating PMS activation.[12] The initial concentration of ENR also affects the degradation of the contaminant. As shown in Figure S19, the degradation efficiency of ENR seemingly decreased with increasing ENR concentration. In terms of the removal rate of ENR, the removal rate of ENR increased from 9.80 to 19.22 $mg \cdot L^{-1} \cdot min^{-1}$ when the concentration of ENR increased from 10 $mg \cdot L^{-1}$ to 40 $mg \cdot L^{-1}$. This may be because high concentrations of ENR had more chance of collision during the limited lifetime time of ROSs.

Figures

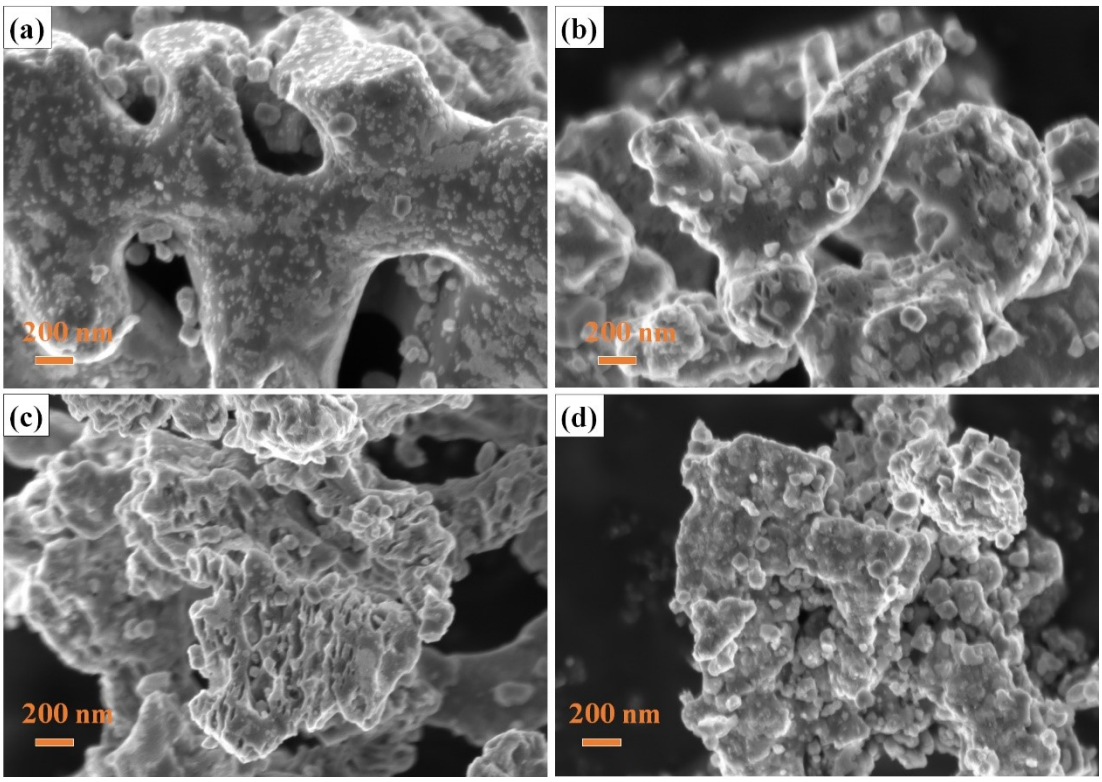

Figure S1. SEM images of the perovskites SC (a), SCC-1 (b) SCC-2 (c), and SCC-3 (d).

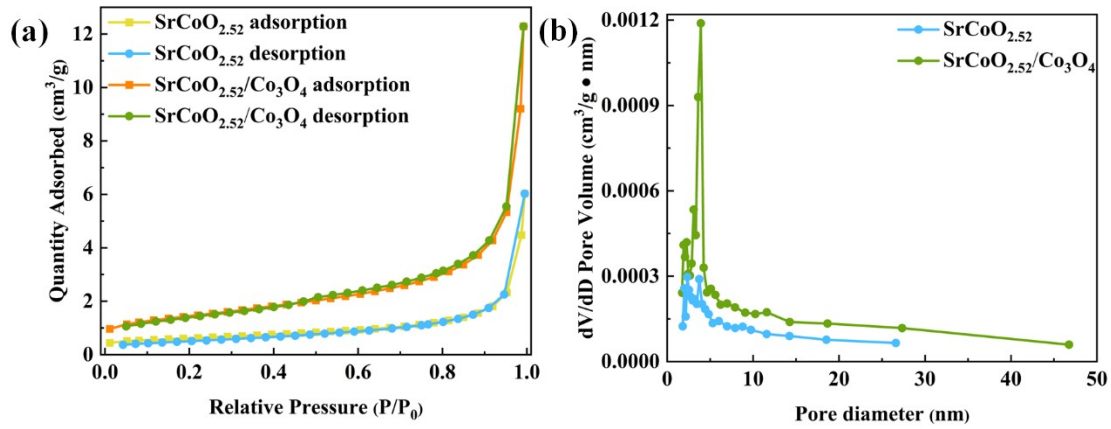

Figure S2. (a) BET specific surface area and (b) BJH average pore diameter for SC and SCC-2.

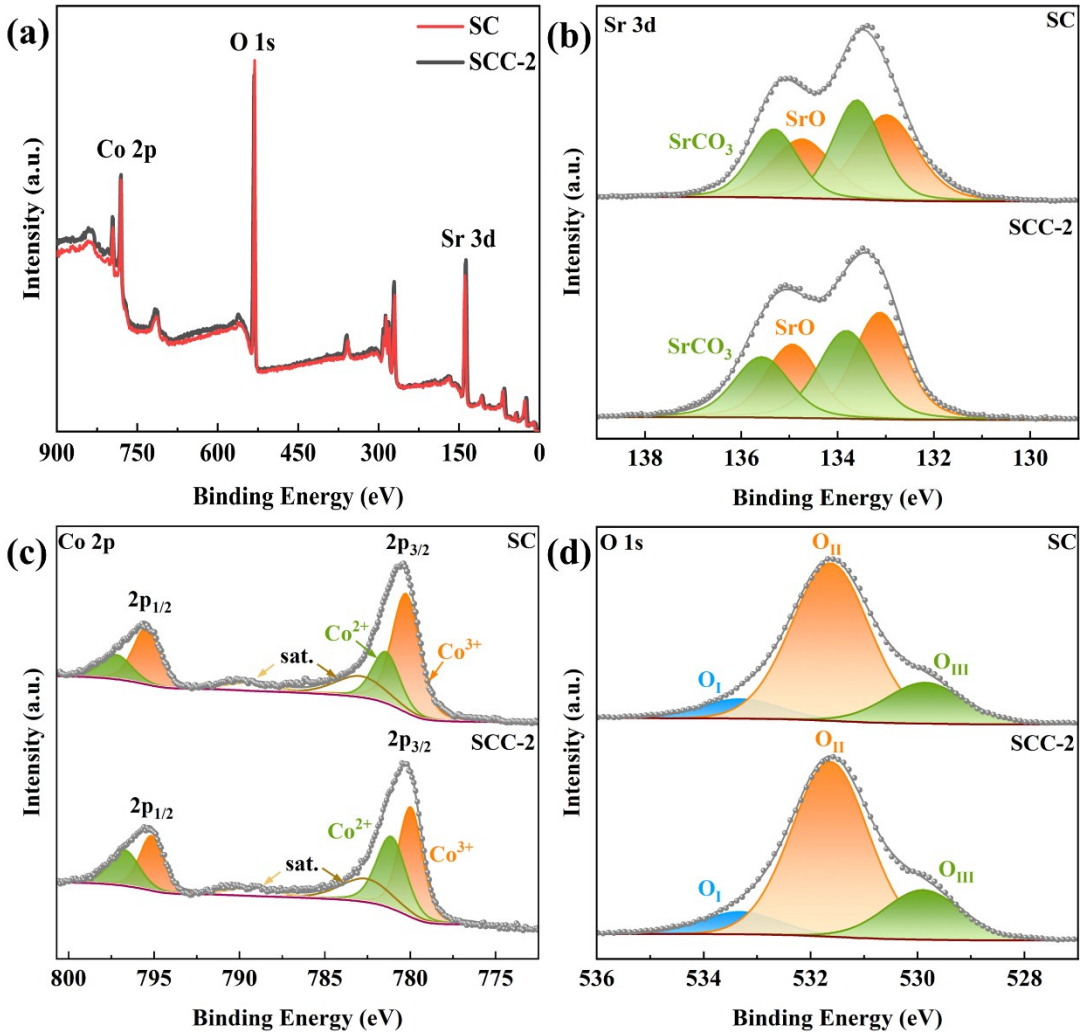

Figure S3. The XPS survey spectra (a); the high-resolution spectra of Sr 3d (b), Co 2p (c), and O 1s (d) in perovskites SC and SCC-2.

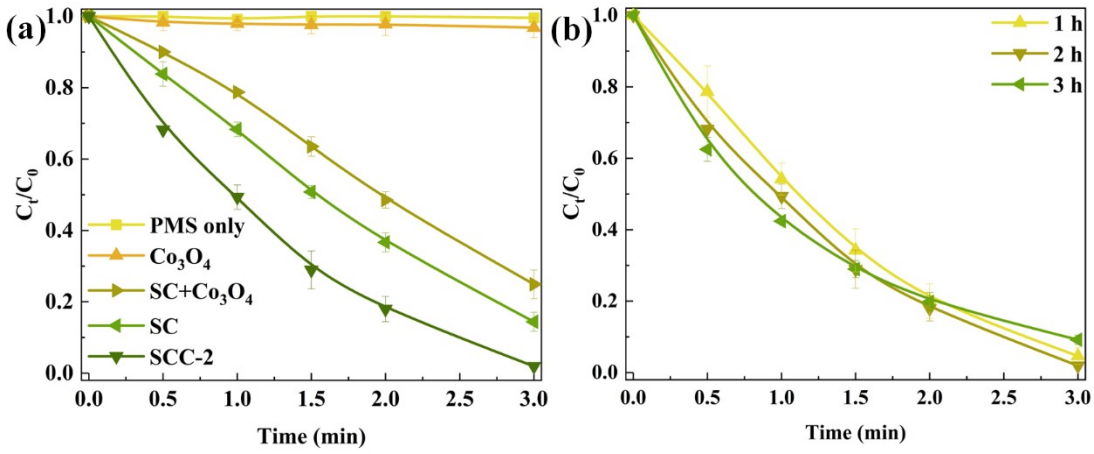

Figure S4. The degradation of ENR in different reaction system (a), and the degradation of ENR in SCC-x/PMS system with different processed time.

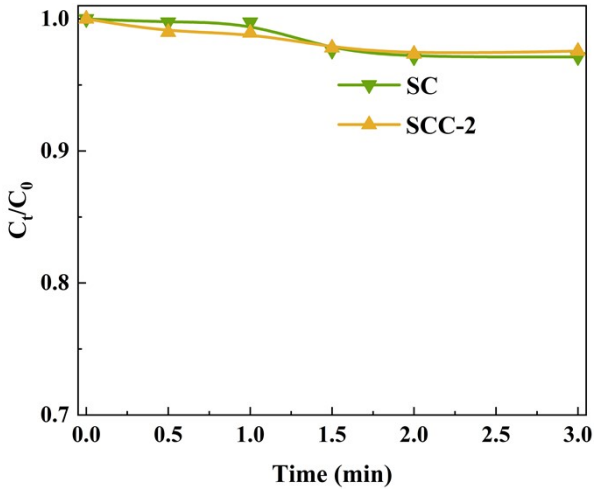

Figure S5. The ENR adsorption efficiency through SC and SCC-2 materials.

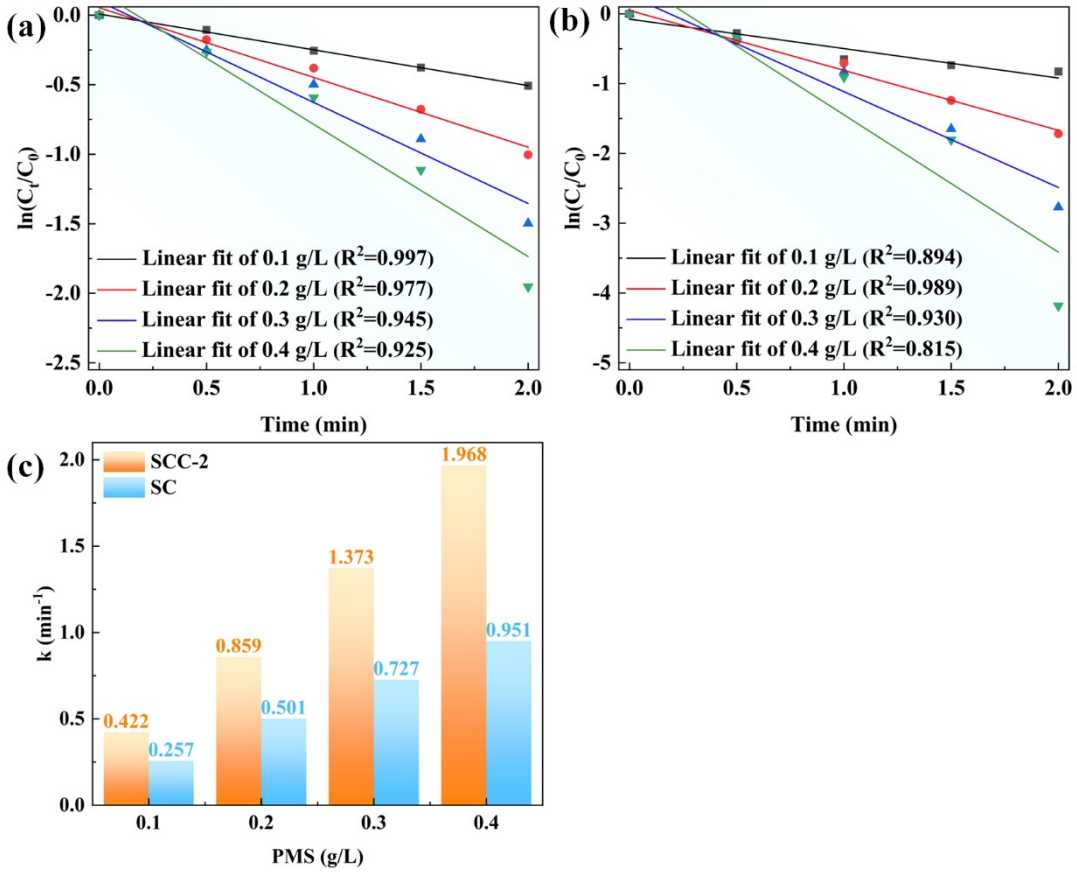

Figure S6. The k_{obs} fitting for SC/PMS (a) and SCC-2/PMS (b) system with different PMS dosage; (c) The k_{obs} value of SC/PMS and SCC-2/PMS system with different PMS dosage.

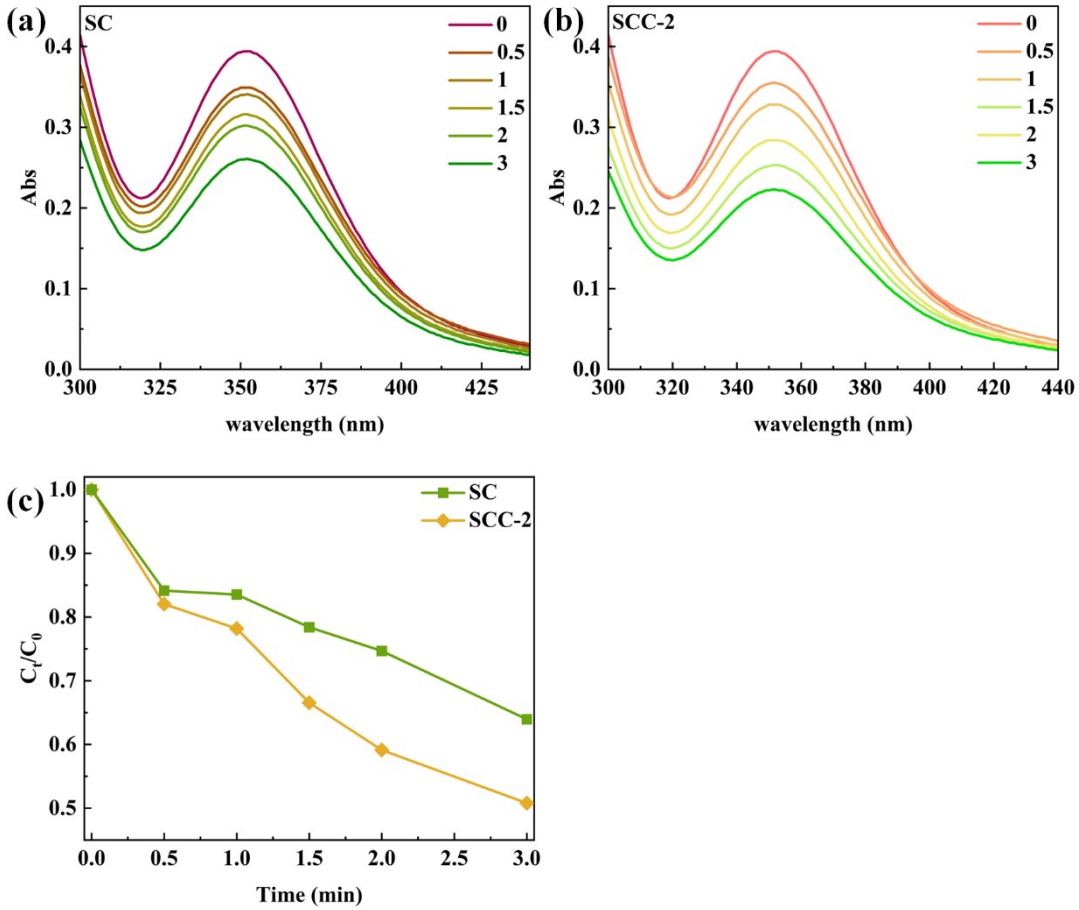

Figure S7. The absorbance of PMS in SC/PMS (a) and SCC-2/PMS (b) system; (c) the residual rate of PMS in SC/PMS and SCC-2/PMS system.

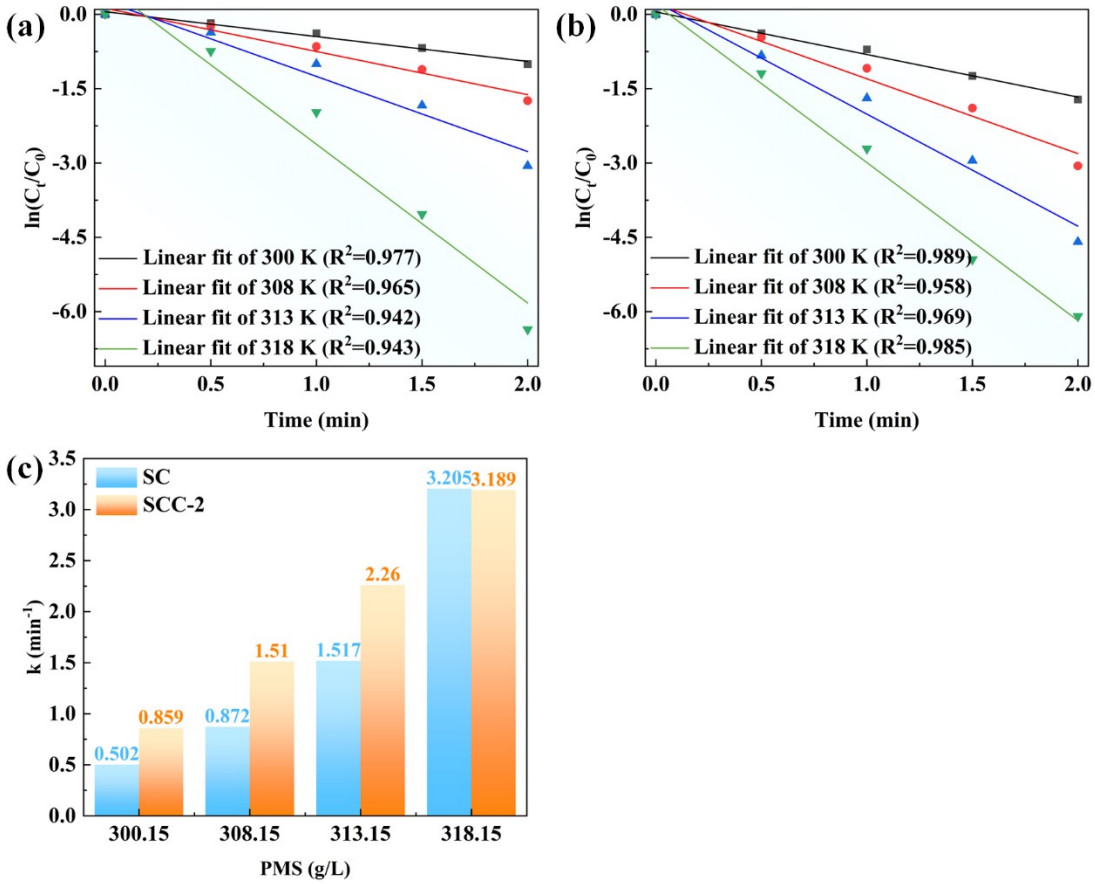

Figure S8. The k_{obs} fitting for SC/PMS (a) and SCC-2/PMS (b) system with different temperature; (c) The k_{obs} value of SC/PMS and SCC-2/PMS system with different temperature.

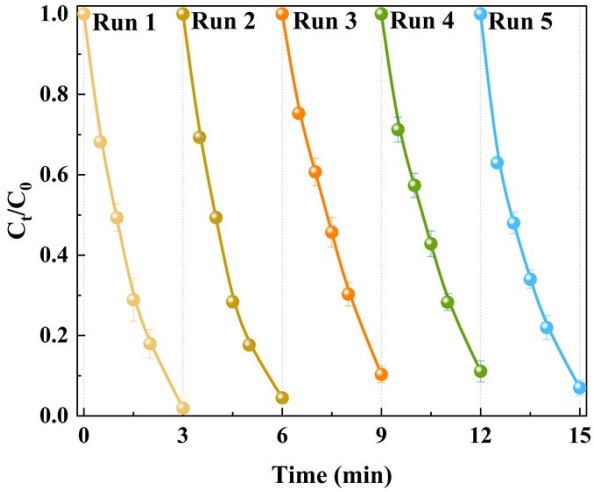

Figure S9. The degradation of ENR in SCC-2/PMS system for five cycles.

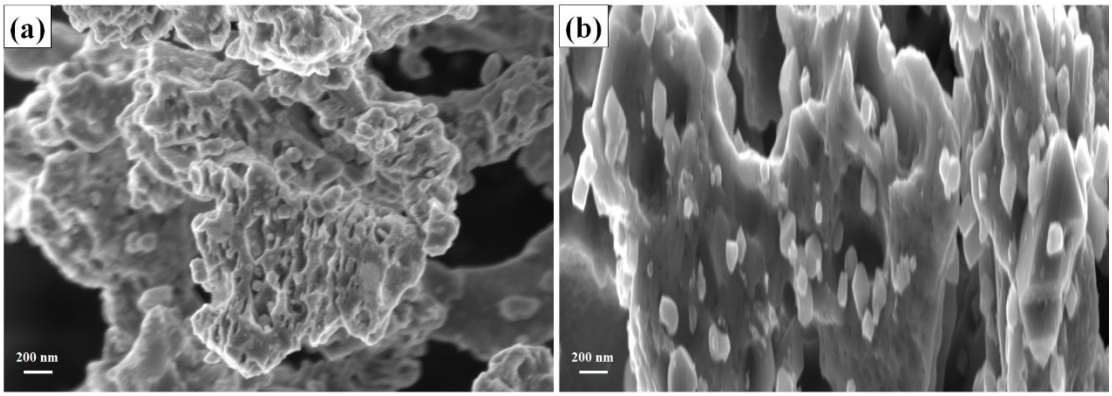

Figure S10. The SEM images of SCC-2 before (a) and after (b) reaction

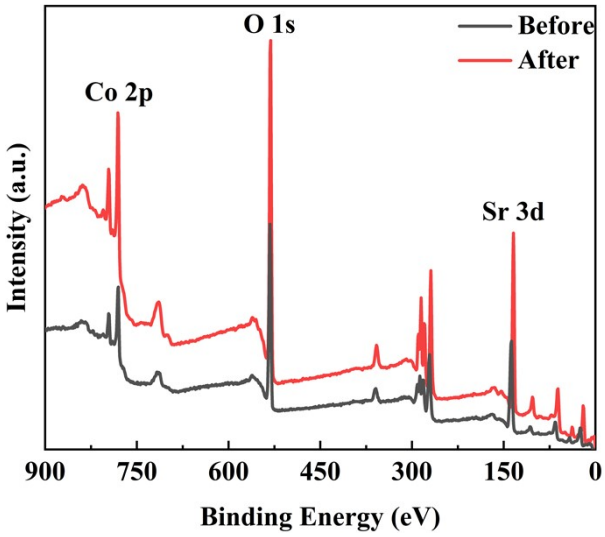

Figure S11. The XPS survey spectra of SCC-2 before and after reaction.

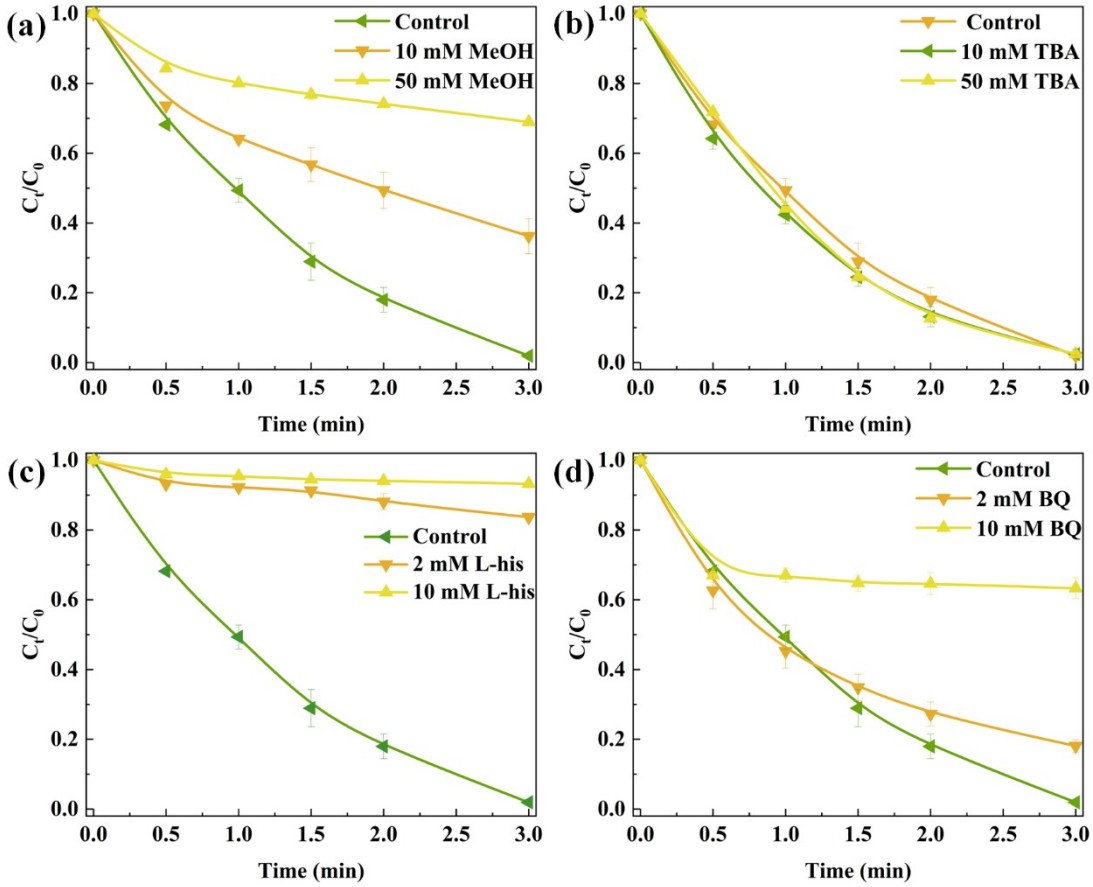

Figure S12. The ENR degradation in (a) MeOH, (b) TBA, (c) L-his, and (d) BQ scavenger systems.

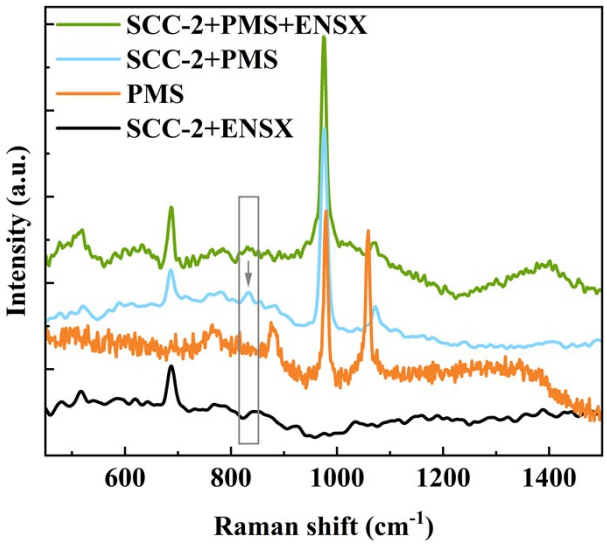

Figure S13. The Raman spectra of various SCC-2 suspensions

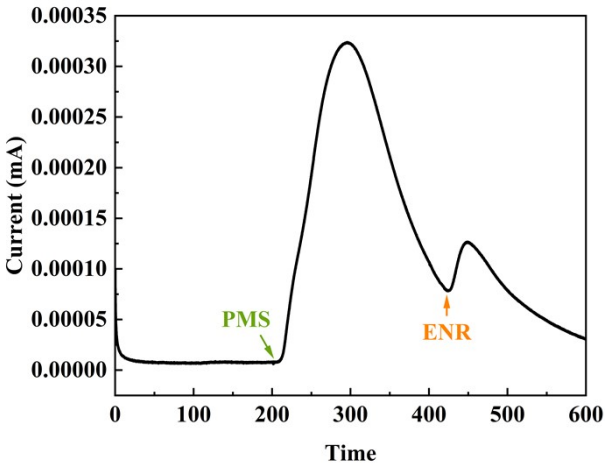

Figure S14. I-t curves upon the addition of PMS and ENR.

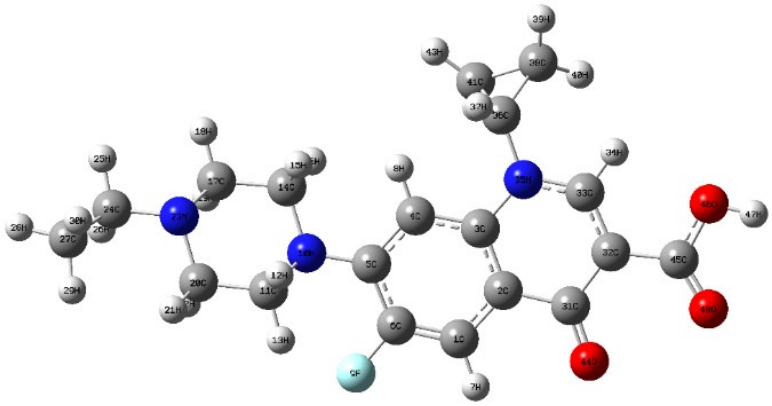

Figure S15. ENR molecule structure

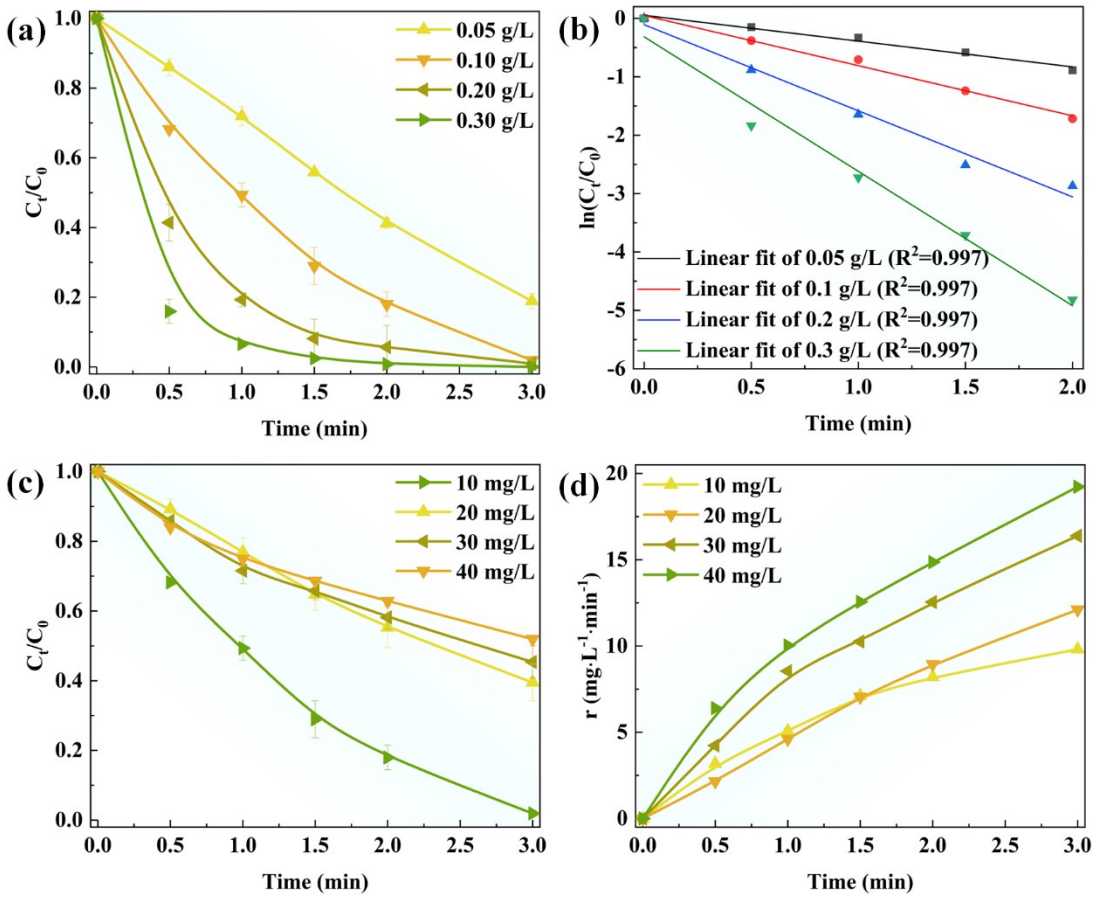

Figure S16. The degradation of ENR (a) and the k_{obs} fitting (b) in SCC-2/PMS system with different SCC-2 dosage; (c) the degradation of ENR in SCC-2/PMS system with different SCC-2 concentration.

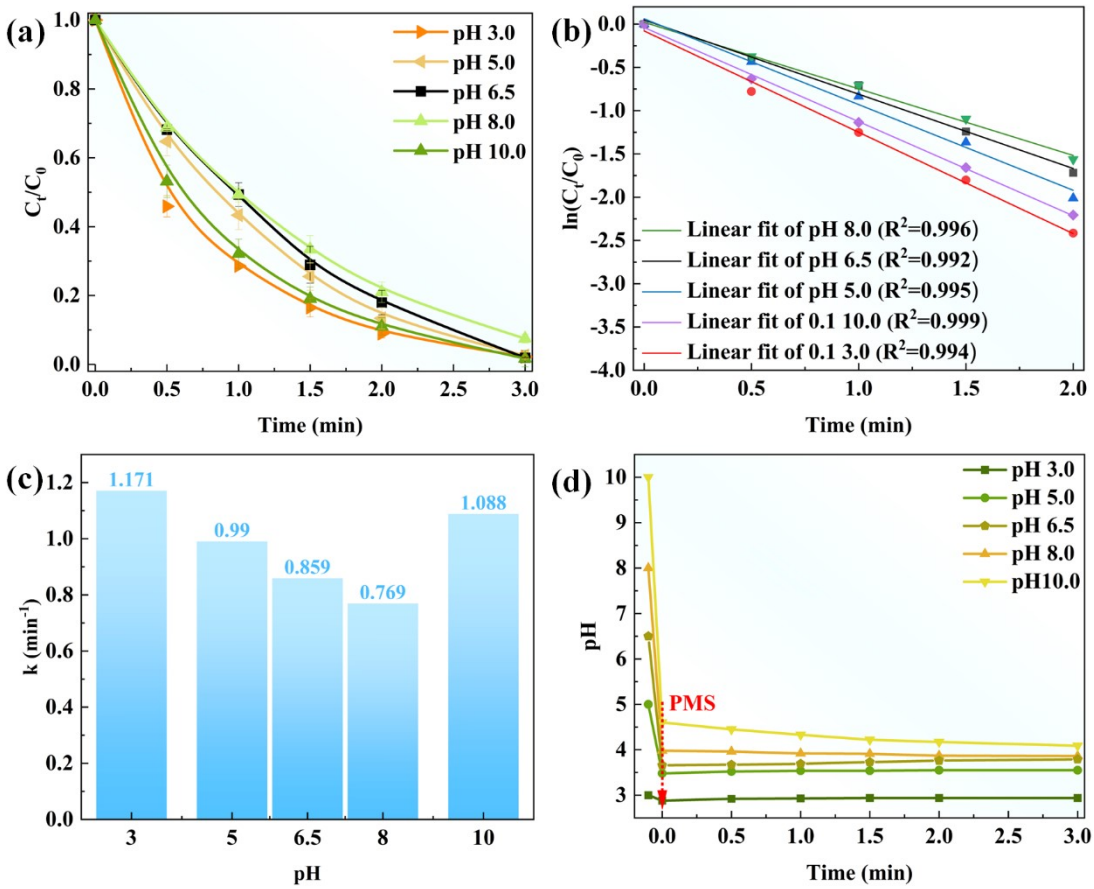

Figure S17. The degradation of ENR (a), the k_{obs} fitting (b), and the k_{obs} value in SCC-2/PMS system with different pH; the pH change in SCC-2/PMS system.

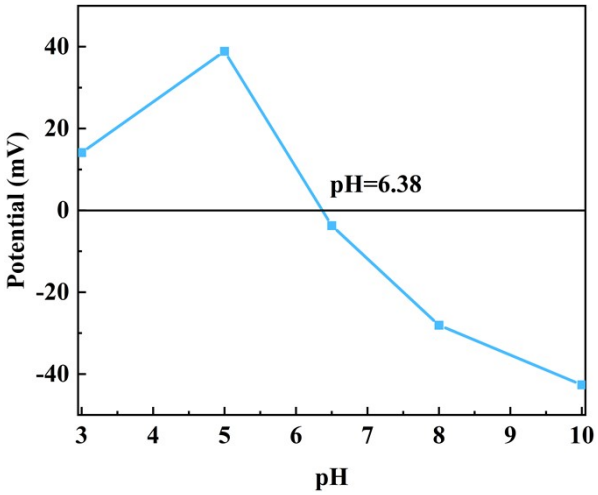

Figure S18. The zeta potential of SCC-2 at different pH.

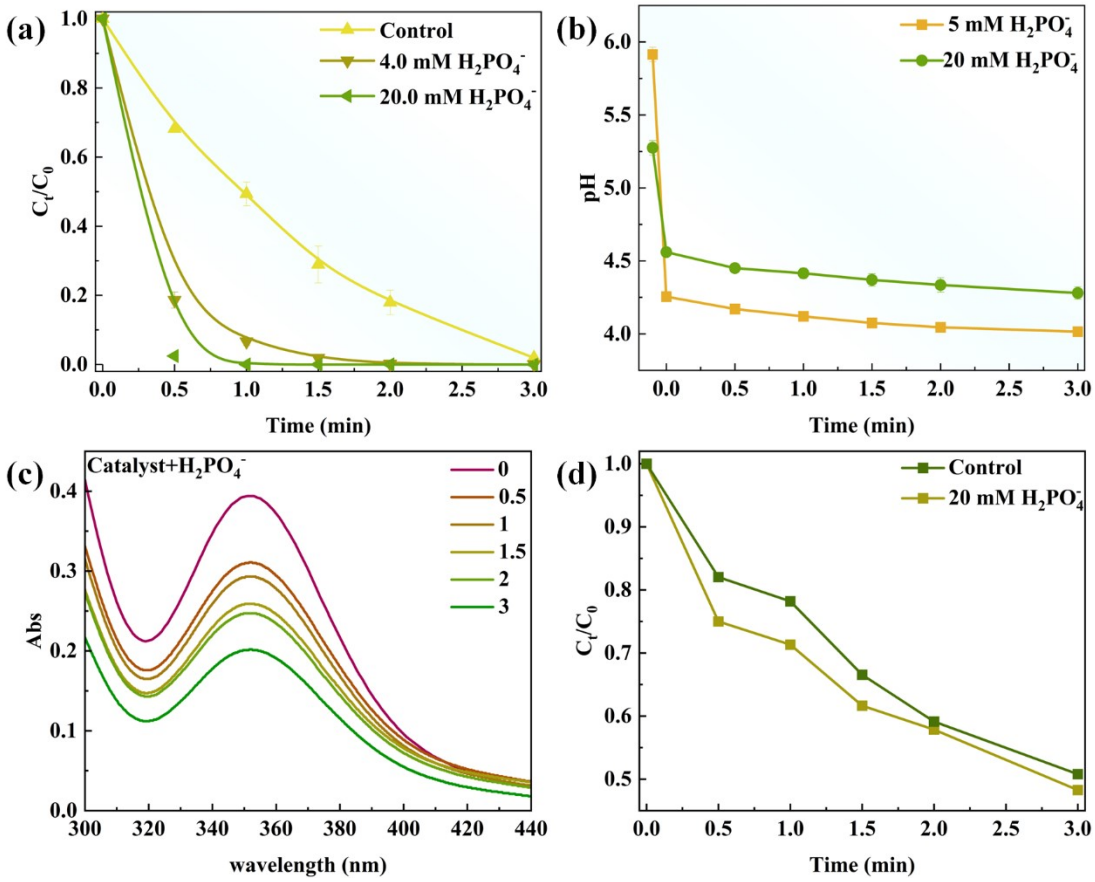

Figure S19. (a) The degradation of ENR in SCC-2/PMS system with $H_2PO_4^-$, (b) the pH change in SCC-2/PMS system with addition of $H_2PO_4^-$, (c) the absorbance of PMS in SCC-2/PMS system with addition of $H_2PO_4^-$, and (d) the residual rate of PMS in SCC-2/PMS system with and without $H_2PO_4^-$.

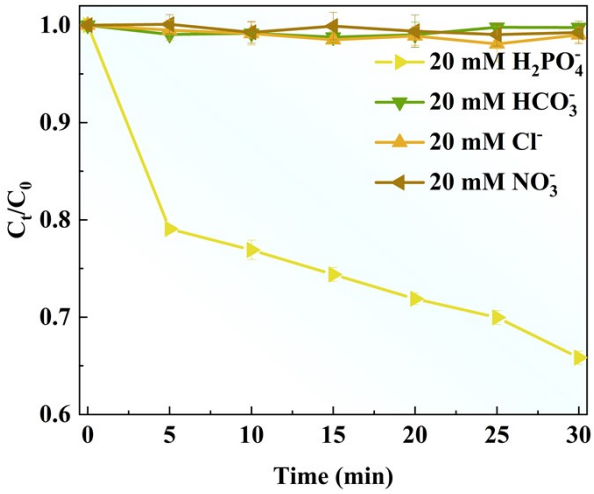

Figure S20. The ENR adsorption efficiency through SCC-2 materials with different anions.

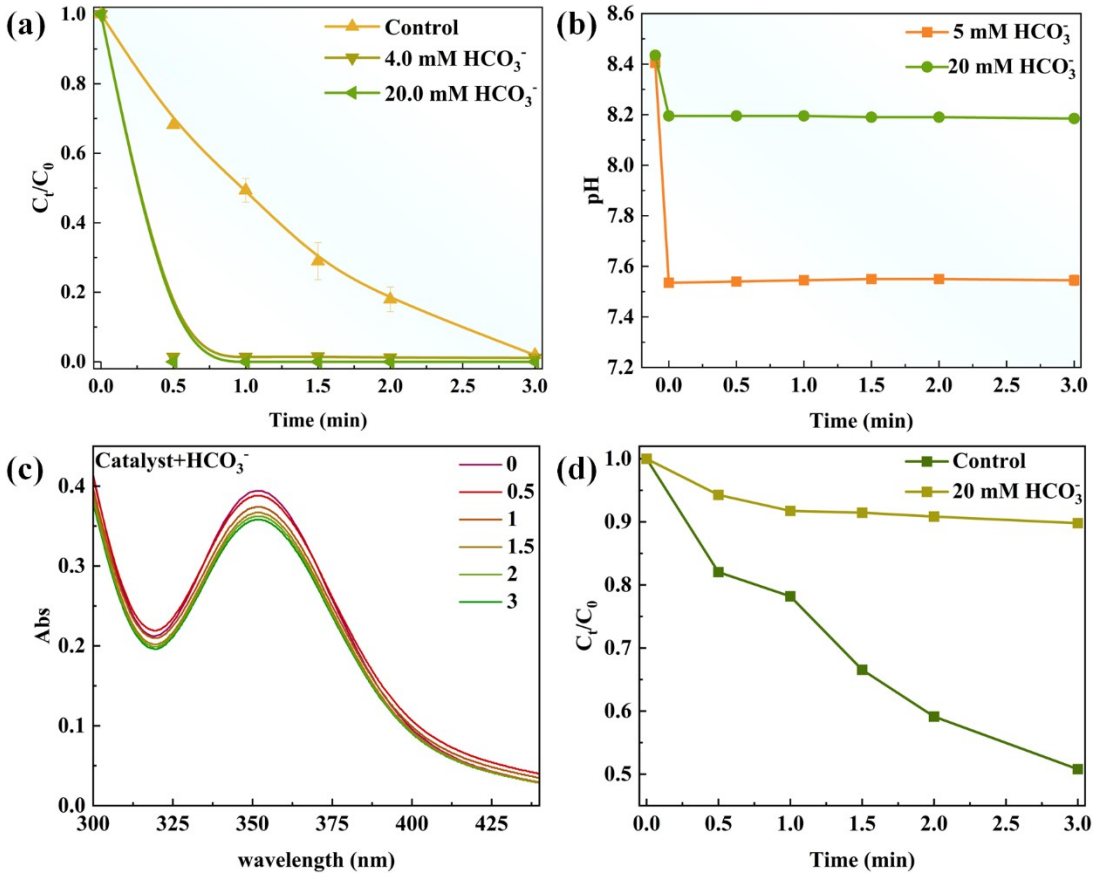

Figure S21. (a) The degradation of ENR in SCC-2/PMS system with HCO_3^-, (b) the pH change in SCC-2/PMS system with addition of HCO_3^-, (c) the absorbance of PMS in SCC-2/PMS system with addition of HCO_3^-, and (d) the residual rate of PMS in SCC-2/PMS system with and without HCO_3^-.

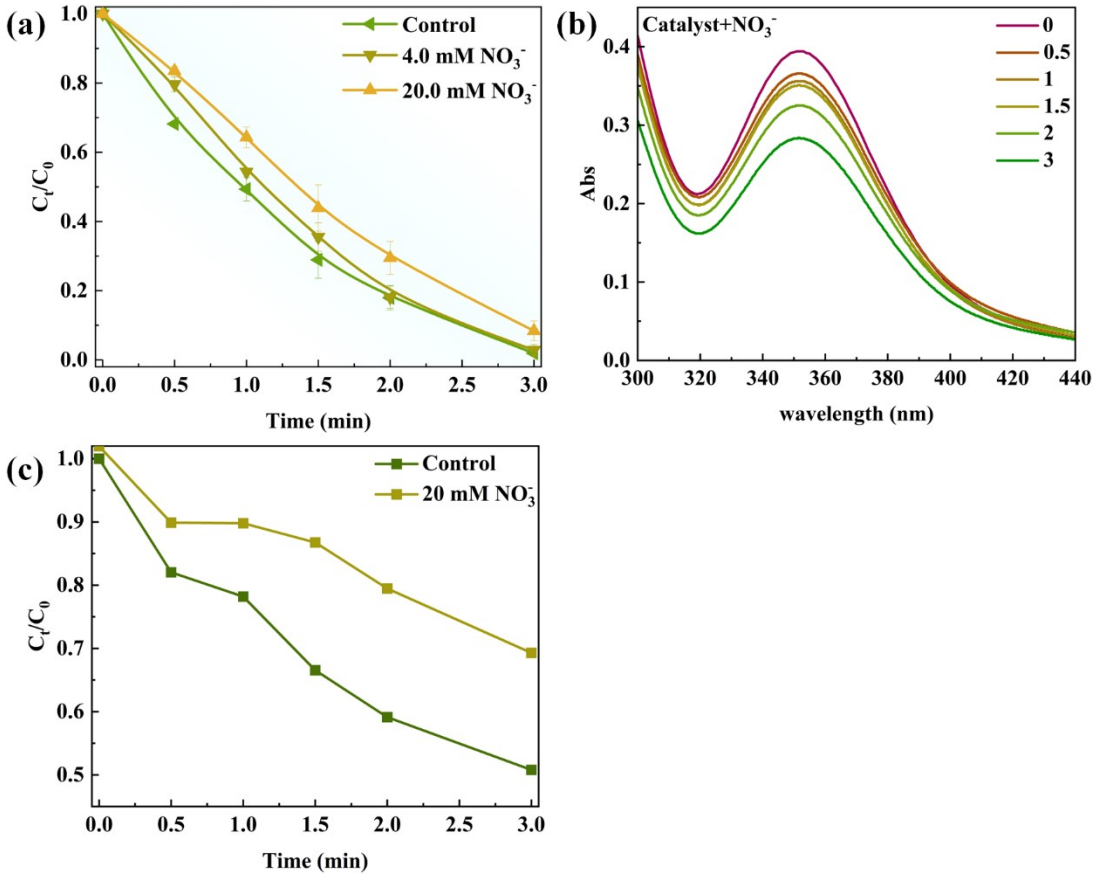

Figure S22. (a) The degradation of ENR in SCC-2/PMS system with NO_3^-, (b) the absorbance of PMS in SCC-2/PMS system with addition of NO_3^-, and (c) the residual rate of PMS in SCC-2/PMS system with and without NO_3^-.

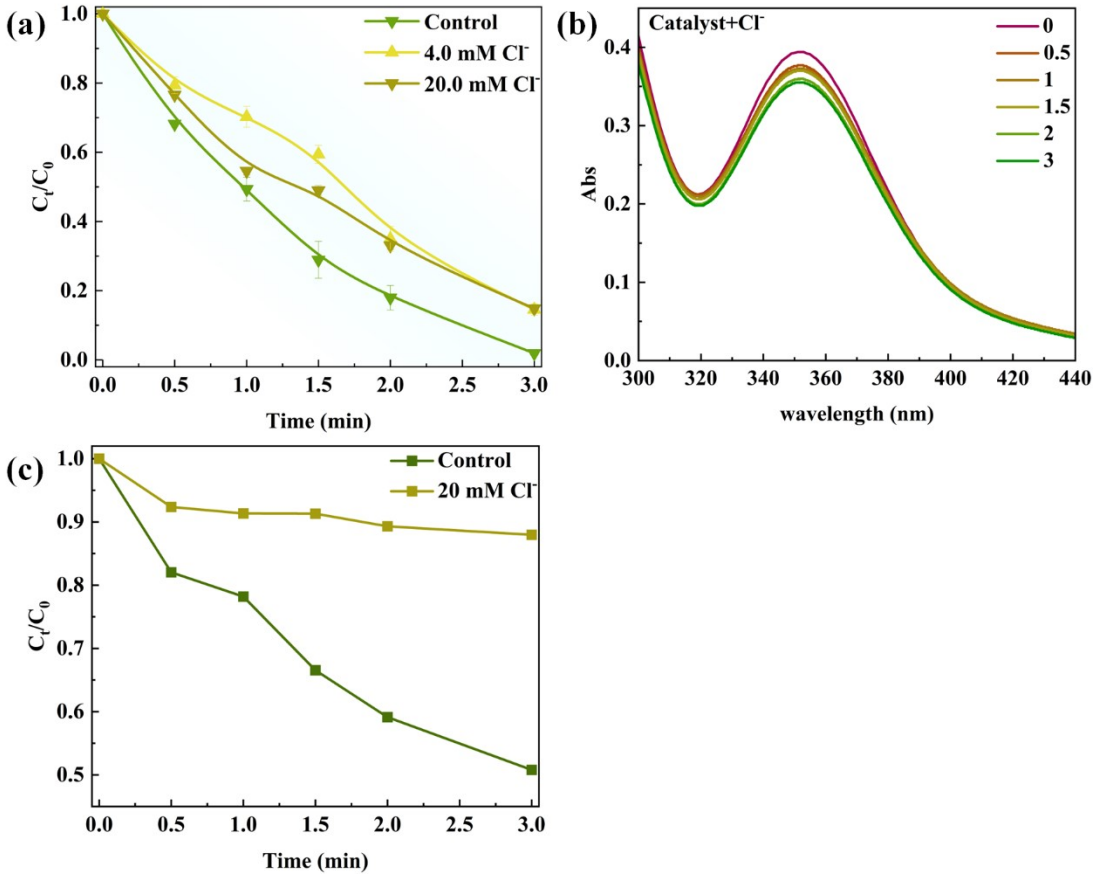

Figure S23. (a) The degradation of ENR in SCC-2/PMS system with Cl^-, (b) the absorbance of PMS in SCC-2/PMS system with addition of Cl^-, and (c) the residual rate of PMS in SCC-2/PMS system with and without Cl^-.

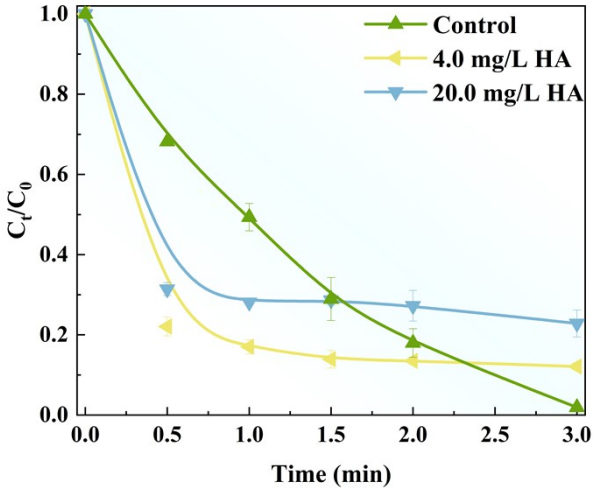

Figure S24. The degradation of ENR in SCC-2/PMS system with HA.

Tables

Table S1. The Sr and Co content of perovskite SC and SC-x through inductively coupled plasma mass spectrometry (ICP-MS).

samples	Co content (W %)	Co content (mol %)	Sr content (W %)	Sr content (mol %)	atomic ratio of Sr/Co
SC	31.39%	0.0053	47.56%	0.0054	0.98
SC-1	34.33%	0.0058	42.52%	0.0049	0.83
SC-2	35.70%	0.0061	39.90%	0.0046	0.75
SC-3	39.17%	0.0067	39.19%	0.0045	0.67

Table S2. The adsorption energies of PMS on the SC and SCC-2 surface at different sites.

adsorption energy	Sr site (eV)	Co site (eV)	O site (eV)
SC	-3.254149644	-2.572936307	-0.079181312
SCC-2	_	-0.730064765	0.054495722

Table S3. Natural population analysis (NPA) charge distribution and Fukui index (f^-, f^+, and f^0) of ENR.

Atom	q(N)	q(N+1)	q(N-1)	f-	f+	f0	CDD
1(C)	-0.0381	-0.0942	-0.0279	0.0101	**0.0561**	**0.0331**	0.046
2(C)	-0.0289	-0.0356	-0.0154	0.0135	0.0068	0.0101	-0.0067
3(C)	0.041	0.0304	0.0569	0.0159	0.0106	0.0133	-0.0053
4(C)	-0.0776	-0.1302	-0.0625	0.0151	**0.0527**	**0.0339**	0.0376
5(C)	0.0408	-0.0028	0.0585	0.0177	**0.0436**	**0.0307**	0.0259
6(C)	0.0858	0.0427	0.1052	0.0194	**0.0432**	**0.0313**	0.0238
7(H)	0.0612	0.0338	0.073	0.0118	0.0274	0.0196	0.0156
8(H)	0.0341	0.0123	0.0445	0.0104	0.0217	0.0161	0.0113
9(F)	-0.0952	-0.129	-0.0751	**0.0201**	**0.0338**	0.0269	0.0136
10(N)	-0.0769	-0.0923	-0.0671	0.0098	0.0154	0.0126	0.0057
11(C)	-0.0078	-0.0139	-0.0019	0.0059	0.0061	0.006	0.0001
12(H)	0.0237	0.0147	0.0332	0.0096	0.009	0.0093	-0.0006
13(H)	0.0363	0.0324	0.0452	0.0089	0.0039	0.0064	-0.005
14(C)	-0.0053	-0.0092	-0.0001	0.0052	0.0039	0.0046	-0.0014
15(H)	0.0231	0.0164	0.0315	0.0084	0.0066	0.0075	-0.0018
16(H)	0.0371	0.0346	0.0468	0.0097	0.0025	0.0061	-0.0072
17(C)	-0.0105	-0.0149	0.0037	0.0142	0.0044	0.0093	-0.0098
18(H)	0.035	0.025	0.0517	0.0167	0.01	0.0133	-0.0067
19(H)	0.019	0.0126	0.0441	**0.0251**	0.0063	0.0157	-0.0188
20(C)	-0.0108	-0.0153	0.0032	0.0141	0.0045	0.0093	-0.0096
21(H)	0.0375	0.0277	0.0535	0.0159	0.0098	0.0129	-0.0061
22(H)	0.0197	0.0137	0.0444	**0.0247**	0.0059	0.0153	-0.0188
23(N)	-0.1117	-0.1127	-0.0289	**0.0828**	0.001	**0.0419**	-0.0818
24(C)	-0.0053	-0.0089	0.0081	0.0134	0.0036	0.0085	-0.0099
25(H)	0.0311	0.0253	0.0454	0.0143	0.0057	0.01	-0.0085
26(H)	0.0158	0.0105	0.0413	**0.0255**	0.0054	0.0154	-0.0201
27(C)	-0.0876	-0.0912	-0.0795	0.0081	0.0036	0.0059	-0.0045
28(H)	0.0348	0.0261	0.0505	0.0157	0.0087	0.0122	-0.007
29(H)	0.0306	0.0283	0.0376	0.007	0.0024	0.0047	-0.0047
30(H)	0.0329	0.0297	0.0416	0.0087	0.0032	0.0059	-0.0055
31(C)	0.1107	0.06	0.147	**0.0363**	**0.0507**	**0.0435**	0.0144
32(C)	-0.0575	-0.0977	-0.0379	0.0196	**0.0402**	**0.0299**	0.0206
33(C)	0.0384	-0.072	0.068	**0.0296**	**0.1104**	**0.07**	0.0808
34(H)	0.0522	0.0121	0.0714	0.0192	**0.0401**	**0.0296**	0.0208
35(N)	0.0025	-0.0298	0.0255	**0.023**	0.0324	**0.0277**	0.0094
36(C)	0.0197	0.0191	0.0199	0.0001	0.0007	0.0004	0.0006
37(H)	0.0493	0.0319	0.0586	0.0093	0.0175	0.0134	0.0082
38(C)	-0.061	-0.0758	-0.0503	0.0107	0.0148	0.0128	0.004
39(H)	0.0521	0.0332	0.0648	0.0127	0.0189	0.0158	0.0062

40(H)	0.0531	0.0443	0.0583	0.0052	0.0088	0.007	0.0037
41(C)	-0.065	-0.0789	-0.0568	0.0082	0.0139	0.011	0.0057
42(H)	0.052	0.0448	0.0556	0.0036	0.0072	0.0054	0.0035
43(H)	0.0486	0.0309	0.058	0.0094	0.0178	0.0136	0.0084
44(O)	-0.2834	-0.3647	-0.0995	**0.1839**	**0.0813**	**0.1326**	-0.1026
45(C)	0.1942	0.1666	0.2175	**0.0232**	**0.0276**	0.0254	0.0043
46(O)	-0.1945	-0.2147	-0.1573	**0.0372**	0.0202	**0.0287**	-0.017
47(H)	0.1838	0.1586	0.2074	**0.0236**	0.0252	0.0244	0.0016
48(O)	-0.2789	-0.3337	-0.2115	**0.0673**	**0.0549**	**0.0611**	-0.0125

Table S4. Accurate Mass Measurement of ENR Degradation Products Using LTQ Oribitrap Velos Electrospray Ionization in Positive Ion Mode

Theo. mass	Formula	$[M+H]^+$ (m/z)	RT	Delta (ppm)	RDB
ENR=359.16452	$C_{19}H_{12}FN_3O_3$	360.17075	4.16	-2.92	9.5
P1=377.13870	$C_{18}H_{20}FN_3O_5$	378.14481	5.53	-3.09	9.5
P4=361.14378	$C_{18}H_{20}FN_3O_4$	362.14978	3.88	-3.54	9.5
P2/P9=349.14378	$C_{17}H_{20}FN_3O_4$	350.14999	4.64	-3.05	8.5
P5=333.14887	$C_{17}H_{20}FN_3O_3$	334.15515	4.09	-2.98	8.5
P3/P6/P10=321.11248	$C_{15}H_{16}FN_3O_4$	322.11976	4.25	-2.68	8.5
P7=234.08519	$C_8H_{14}N_2O_6$	235.09181	4.32	-2.77	2.5
P11=148.01604	$C_8H_4O_3$	149.01940	4.00	-2.08	6.5
P8=121.07389	$C_4H_{11}NO_3$	122.08106	3.83	0.88	-0.5

References

1. W. Xie, G. Y. Xu, Y. Zhang, Y. B. Yu and H. He, *J. Hazard. Mater.*, 2022, **431**, 128528.
2. X. Y. Mi, H. Zhong, H. X. Zhang, S. Z. Xu, Y. Li, H. T. Wang, S. H. Zhan and J. C. Crittenden, *Environ. Sci. Technol.*, 2022, **56**, 2637-2646.
3. J. F. Yu, L. Tang, Y. Pang, G. M. Zeng, H. P. Feng, J. J. Zou, J. J. Wang, C. Y. Feng, X. Zhu, X. L. Ouyang and J. S. Tan, *Appl. Catal., B*, 2020, **260**, 118160.
4. X. Li, C. Xiao, X. Ruan, Y. Y. Hu, C. Y. Zhang, J. H. Cheng and Y. C. Chen, *Chem. Eng. J.*, 2022, **427**, 130927.
5. J. B. An, Y. L. Li, W. Chen, G. Q. Li, J. H. He and H. X. Feng, *Environ. Res.*, 2020, **191**, 110067.
6. C. J. Liang, C. F. Huang, N. Mohanty and R. M. Kurakalva, *CHEMOSPHERE*, 2008, **73**, 1540-1543.
7. J. Hutter, M. Iannuzzi, F. Schiffmann and J. VandeVondele, *Wiley Interdiscip. Rev.: Comput. Mol. Sci.*, 2014, **4**, 15-25.
8. G. Lippert, J. Hutter and M. Parrinello, *Mol. Phys.*, 1997, **92**, 477-487.
9. S. Goedecker, M. Teter and J. Hutter, *PHYSICAL REVIEW B*, 1996, **54**, 1703-1710.
10. S. Grimme, J. Antony, S. Ehrlich and H. Krieg, *J. Chem. Phys.*, 2010, **132**, 3382344.
11. G. Henkelman, B. P. Uberuaga and H. Jonsson, *J. Chem. Phys.*, 2000, **113**, 9901-9904.
12. H. X. Chen, Y. Xu, K. M. Zhu and H. Zhang, *Appl. Catal., B*, 2021, **284**, 119732.